Journal of Magnetic Resonance 203 (2010) 190–198

Contents lists available at ScienceDirect

Journal of Magnetic Resonance

journal homepage: www.elsevier.com/locate/jmr

Communication

Guidelines for the use of band-selective radiofrequency pulses in hetero-nuclear NMR: Example of longitudinal-relaxation-enhanced BEST-type ^{1}H–^{15}N correlation experiments

Ewen Lescop [b], Thomas Kern [a], Bernhard Brutscher [a,*]

[a] Institut de Biologie Structurale – Jean Pierre Ebel C.N.R.S.-C.E.A.-UJF, 41, rue Jules Horowitz, 38027 Grenoble Cedex, France
[b] Centre de Recherche CNRS de Gif-sur-Yvette, Institut de Chimie des Substances Naturelles, Laboratoire de Chimie et Biologie Structurales, 1, avenue de la Terrasse, 91198 Gif-sur-Yvette, France

ARTICLE INFO

Article history:
Received 28 August 2009
Revised 27 November 2009
Available online 4 December 2009

Keywords:
Fast NMR
Proteins
Nucleic acids
Selective pulses
Pulse shaping
Longitudinal relaxation enhancement
HSQC
TROSY

ABSTRACT

Band-selective radiofrequency (rf) pulses provide powerful spectroscopic tools for many biomolecular NMR applications. Band-selectivity is commonly achieved by pulse shaping where the rf amplitude and phase are modulated according to a numerically optimized function. This results in complex spin evolution trajectories during the pulse duration. Here we introduce simplified representations of a number of shaped pulses, commonly used in biomolecular NMR spectroscopy. These simple schemes, consisting in a suite of free evolution delays and ideal rf pulses, reproduce astonishingly well the effect on a scalar-coupled hetero-nuclear two-spin system. As a consequence, optimal use of such pulse shapes in complex multi-pulse sequences becomes straightforward, as demonstrated here for the example of longitudinal-relaxation-enhanced BEST-HSQC and BEST-TROSY experiments. Applications of these optimized pulse sequences to several proteins in the size range of 8–21 kDa are shown.

1. Introduction

A particularly nice feature of Nuclear Magnetic Resonance (NMR) is that the pulse sequences, required to perform various coherence–transfer pathways can be designed from very simple principles despite the quantum mechanical nature of the manipulated spin system. Herein, we will focus on liquid-state NMR spectroscopy, although the concepts presented equally apply to solid-state NMR spectroscopy and magnetic resonance imaging (MRI). Unitary spin transformations in weakly coupled spin systems can be described by a series of three-dimensional rotations in product operator space [1]. These simple concepts that form the basis of hundreds of NMR experiments designed for various chemical and biochemical applications, only apply as long as chemical shift and spin-coupling evolution during radiofrequency (rf) pulses can be safely neglected. This is generally the case for "hard" pulses, characterized by a constant high rf power, and a short overall duration of a few microseconds. The situation is more complicated for shaped rf pulses optimized for frequency-selective, or broad-band spin manipulation that are frequently used in a wide range of biomolecular NMR experiments. Generally, homo- and hetero-nuclear spin-coupling evolution during the pulse has not been taken into account for the shape optimization. Therefore, the much longer pulse durations, required to achieve selectivity, together with weak rf amplitudes may result in non negligible *J*-coupling evolution during the shaped pulse. An additional problem associated with shaped pulses is that they have been optimized for a particular purpose (spin rotation) such as *spin excitation* ($I_z \rightarrow I_{xy}$), or *spin inversion* ($I_z \rightarrow -I_z$), while no specification has been made for the effect of the pulse on other initial spin states. So called *general* or *universal* rotation pulse shapes that yield similar rotation properties in spin space than hard pulses have also been designed for certain purposes. In practice, however, they are often more sensitive (than single-rotation pulses) to pulse imperfections, such as B_1 field inhomogeneity or rf miscalibration. For these reasons it may be a non-trivial task to replace hard pulses by shaped pulses in common pulse sequences to make them either band-selective or broad-band. Here, we will be interested in longitudinal-relaxation-enhanced NMR experiments, recently introduced for the study of biological macromolecules, proteins and nucleic acids, that yield an advantage in terms of experimental sensitivity and minimal overall experimental times compared to conventional pulse schemes. Longitudinal relaxation enhancement [2–4] is

* Corresponding author. Address: Laboratoire de RMN, Institut de Biologie Structurale – Jean Pierre Ebel, 41, rue Jules Horowitz, 38027 Grenoble Cedex 1, France.
E-mail address: bernhard.brutscher@ibs.fr (B. Brutscher).

1090-7807/$ - see front matter © 2009 Elsevier Inc. All rights reserved.
doi:10.1016/j.jmr.2009.12.001

based on the selective manipulation of a subset of proton spins, while leaving all other protons close to their thermodynamic equilibrium state. One possible way of selecting a subset of proton spins is by the use of band-selective rf pulses that have been optimized to yield a "top hat" response in frequency (chemical shift offset) space that is uniform (constant rotation angle) over the chosen band width (*excitation/inversion band*), and close to zero (no effect) for spins resonating outside this spectral window. A narrow transition region exists where spin evolution is undefined. Many efforts have been made in the early 90s in developing such band-selective pulses using numerical optimization methods, resulting in a large variety of different pulse shapes. The most popular band-selective pulses used today for biomolecular applications are arguably the BURP pulse family proposed by Geen and Freeman [5], the Gaussian pulse cascades of Emsley and Bodenhausen [6,7], and the SNOB pulses of Kupce et al. [8].

In this communication, we investigate by simulation and experiment the effect of different shaped ^{1}H pulses on an isolated scalar-coupled hetero-nuclear ^{1}H–^{15}N spin system. We demonstrate that the action of certain pulse shapes (ignoring spin relaxation effects) can be approximated by a "binary scheme" consisting in one or two delays, during which ^{1}H chemical shift and hetero-nuclear coupling evolution occurs, and an "ideal" rf pulse accounting for spin rotation around the H_x (or H_y) axis. For practical use, only two very simple binary schemes, a symmetric and an asymmetric one (Fig. 1a), were considered here. A similar concept was recently introduced for the design of broad-band excitation pulses whose effect on the spin system is equivalent to an ideal rf 90° pulse

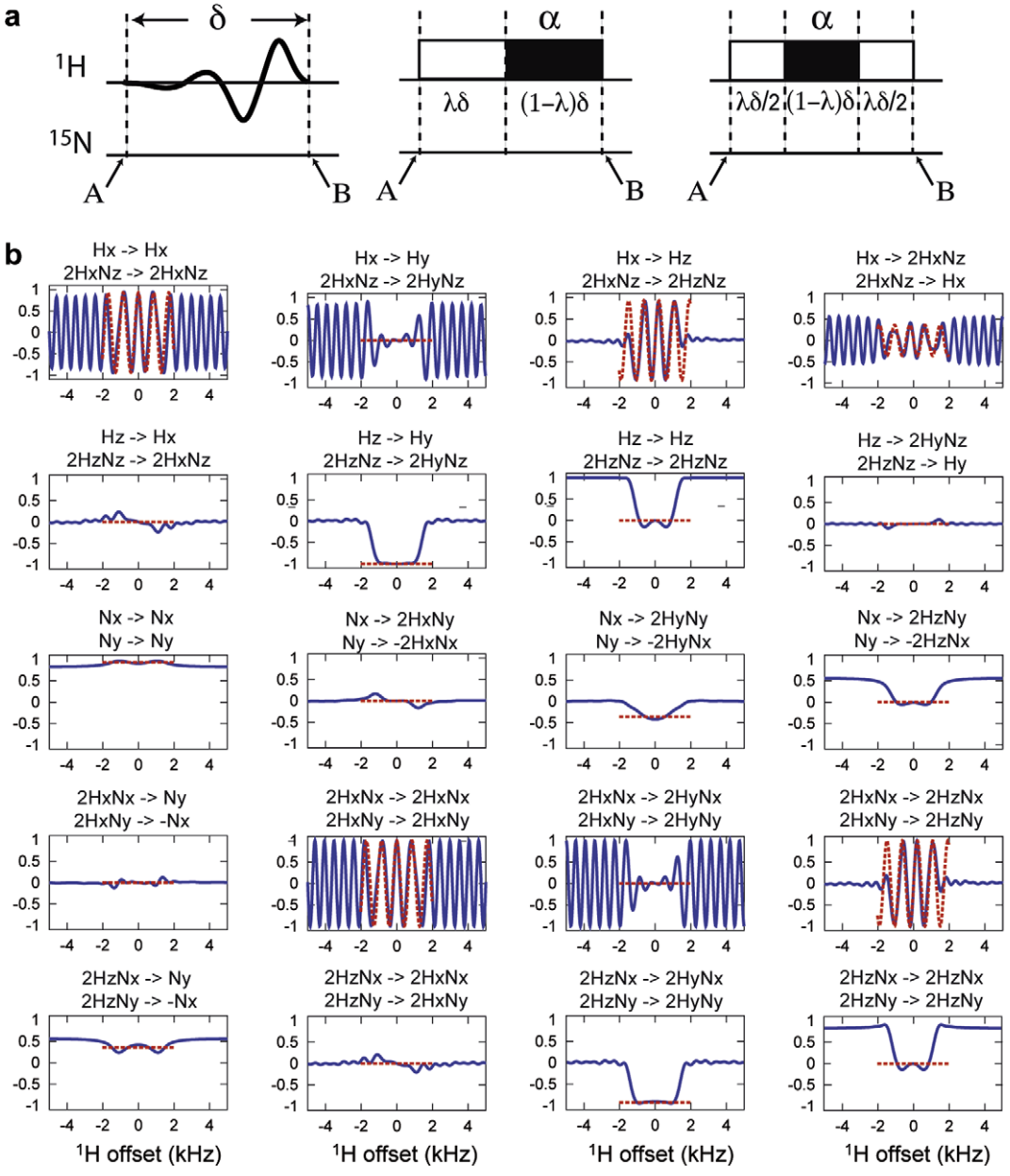

Fig. 1. (a) Asymmetric (center panel) and symmetric (right panel) binary schemes used for the numerical simulations of the effect of a shaped ^{1}H pulse (left panel) on various initial spin states of an isolated scalar-coupled ^{1}H–^{15}N spin system (J_{HN} = 100 Hz). The parameter λ is adjusted to correctly account for chemical shift and spin-coupling evolution during the shaped pulse, while α corresponds to the effective flip angle of the pulse (either 90° or 180°). (b) Selection of representative coherence–transfer pathways computed for EBURP-2 [5] (blue lines) and the corresponding asymmetric binary equivalent (red dashed lines). The EBURP-2 pulse length was set to 1.92 ms corresponding to an excitation bandwidth of about ±1.2 kHz (4 ppm at 600 MHz), and an optimized λ-value of 0.67 was used. (For interpretation of the references to color in this figure legend, the reader is referred to the web version of this article.)

followed by a free evolution delay [9]. Here we propose binary representations for a wide range of band-selective shaped pulses found in the literature. Using these binary (delay/pulse) representations it becomes straightforward to replace standard hard ^{1}H pulses in complex multi-pulse sequences by the appropriate pulse shapes, and to properly adjust transfer and chemical shift editing delays to account for spin evolution during the shaped pulses, even in cases where several coherence–transfer pathways need to be realized at the same time. As an illustration of the method, we will discuss the use of shaped ^{1}H pulses in the context of longitudinal-relaxation-enhanced 2D BEST-HSQC [10,11], and 2D BEST-TROSY [12] pulse schemes, recently developed in our laboratory. The latter is presented here for the first time for protein applications. Although there exists already an abundant literature on shaped pulses and their effect on homo- and hetero-nuclear coupled spin systems (see for example [9,13–15]), we feel that revisiting this topic in the context of recently developed biomolecular NMR experiments will be of practical use for many NMR spectroscopists interested in deriving new pulse schemes, or optimizing well-established correlation experiments replacing hard pulses by appropriate band-selective pulse shapes.

To gain a more detailed understanding of spin evolution during the selective ^{1}H pulses used in BEST-type experiments, we performed calculations for a scalar-coupled ^{1}H–^{15}N spin system using the SPINEVOLUTION software [16]. The simulations of various pulse shapes have been carried out for a ^{1}H Larmor frequency of 600 MHz, a ^{1}H–^{15}N coupling constant of 100 Hz. Spin relaxation during the shaped pulse was not taken into account for the calculation. The effect of a selective pulse on each of the 15 (non-unity) spin states of the density matrix was computed as a function of ^{1}H frequency offset varying from −5 to +5 kHz. ^{15}N offset effects were neglected as the radiofrequency field in the kHz range applied at the Larmor frequency of ^{1}H does not directly affect the ^{15}N spins. Fig. 1b (blue lines) shows the simulation results obtained for an EBURP-2 pulse of duration δ_E = 1.92 ms, yielding spin excitation over a bandwidth of about 4 ppm (2.4 kHz). A total of 40 representative examples, out of the 225 (15×15) possible coherence–transfer pathways are shown. Originally, EBURP-2 has been numerically optimized for performing a $H_z \rightarrow H_y$ rotation over the excitation bandwidth, but interestingly also other coherence–transfer pathways are quite efficient. For example, if applied to transverse ^{1}H coherence H_x or H_y part of the coherence is transferred to H_z spin polarization with an almost linear dependence on the ^{1}H frequency offset. Also some scalar-coupling mediated pathways are observed, e.g. $N_x \rightarrow 2H_yN_y$ and $2H_zN_x \rightarrow N_y$. The observed linear offset-dependence motivated us to search for a suite of 90° general rotation pulse(s) and evolution delays that is able to reproduce the coherence transfer amplitudes achieved by the EBURP-2 pulse within the excitation band. In principle, various binary schemes may account equally well for the density matrix transformation under the shaped pulse, and more complex representations (increasing number of delays and pulses) are expected to yield a better agreement. Here, we only tested the simplest possible binary schemes, depicted in Fig. 1a. The white and black boxes in these schemes represent the fractions of the shaped pulse duration δ during which ^{1}H chemical shift and hetero-nuclear scalar-coupling evolution are active and inactive, respectively. In addition, the black box accounts for the overall rf-induced spin rotation as realized by an ideal band-selective rf pulse of the same length as the black box. Alternatively, this pulse may be viewed as an instantaneous pulse that can be applied at any location within the black-box time interval without affecting the final result. The overall duration of the binary scheme is identical to the shaped pulse length thus ensuring correct description of ^{15}N chemical shift evolution during the shaped pulse. For computational purposes, the white box(es) is (are) replaced by a delay of overall length $\lambda\delta_E$, while the black box is approximated by an instantaneous 90° ^{1}H pulse of the same phase as the shape. The duration of the black box can be neglected as no ^{15}N chemical shift evolution is taken into account for this simulation. The transfer amplitudes computed for the asymmetric binary scheme of Fig. 1a (with α = 90° and λ = 0.67) are plotted in the graphs of Fig. 1b as a function of frequency offset for different pathways (red dashed lines), and superposed on the results obtained for the EBURP-2 pulse (blue lines). The difference in transfer amplitude between the original shape and the simplified binary sequence was evaluated by computing a quality factor Q defined as:

$$Q = \left\{ \frac{\sum_{l=1}^{15}\sum_{k=1}^{15}\left(\sigma_{k;l}^{sh} - \sigma_{k;l}^{bi}\right)^2}{\sum_{l=1}^{15}\sum_{k=1}^{15}\sigma_{k;l}^{sh^2}} \right\}^{\frac{1}{2}} \tag{1}$$

with $\sigma_{k;l}^{sh}$ and $\sigma_{k;l}^{bi}$ the final density matrix elements obtained for the pathway k to l using either the original (amplitude-modulated) pulse shape (*sh*) or its binary replacement scheme (*bi*), and the sums extending over all 15 spin states of the density matrix. This Q factor ranges from 0 for exactly identical transformation to 2 for anti-correlated transformation, while a Q-factor value of 1 indicates the absence of correlation. For each frequency offset $\Delta\Omega$, a Q-factor value $Q(\Delta\Omega)$ is calculated. The mean Q-factor, denoted R, is then used as a measure of how well the binary scheme reproduces the effect of the shaped pulse on the two-spin system over a given frequency interval $[-\omega_{max}, +\omega_{max}]$. R is defined as:

$$R(\omega_{max}) = \frac{1}{2\omega_{max}} \int_{\Delta\Omega=-\omega_{max}}^{+\omega_{max}} Q(\Delta\Omega)d(\Delta\Omega) \tag{2}$$

For simple binary schemes as those introduced in Fig. 1a, a two-dimensional surface $R(\omega_{max}, \lambda)$ is obtained. In order to identify the optimal λ-value, we have set $2\omega_{max}$ to 75% of the excitation bandwidth for which the pulse shape has been initially optimized. The reduced frequency range takes into account that band-selective pulse shapes generally perform less well at the edges of the excitation/inversion region. For the case of a 1.92 ms EBURP-2 pulse resulting in an expected excitation range of 2.4 kHz, a minimal R-value of $R(0.9\text{ kHz}) = 0.14$ was found for λ = 0.67. The good agreement between the real EBURP-2 shape and its binary replacement scheme may also be appreciated from the transfer amplitude profiles shown in Fig. 1b.

Similar calculations as those shown for EBURP-2 in Fig. 1b were done for other shaped pulses commonly used in biomolecular NMR spectroscopy. For all pulse shape simulations, we assumed that no additional ^{15}N pulses are applied simultaneously to the shaped ^{1}H pulse. Refocusing pulses are often encountered in hetero-nuclear pulse sequences with a simultaneous 180° (high-power) ^{15}N pulse applied at the center of the shaped ^{1}H pulse (for example, see Figs. 3–5). In order to investigate the amount of hetero-nuclear coupling evolution during such a pulse sandwich, simulations were done for this class of shapes with the additional 180° ^{15}N pulse. Binary replacement schemes (of the type shown in Fig. 1a) yielding R-values below 0.16 were found for many (but not all) of the shaped pulses. Fig. 2 shows the amplitude-modulated pulse shapes, the numerically optimized binary schemes (and R-values), and the excitation (or inversion) profiles obtained for the excitation (E) pulses EBURP-2 [5], E400B [17], Q5 [7], and PC9 [18], the inversion (I) pulse ISNOB-5 [8], and the refocusing (R) pulses REBURP [5] and Q3 [7]. We also checked that the optimal λ and minimal R-values are independent of the EBURP-2 pulse length (within a range of ±50%), indicating that the results presented here are equally valid for other experimental conditions (magnetic field strengths and excitation bandwidths) as those considered here. All these pulse shapes can also be applied time-reversed. In particular, a time-

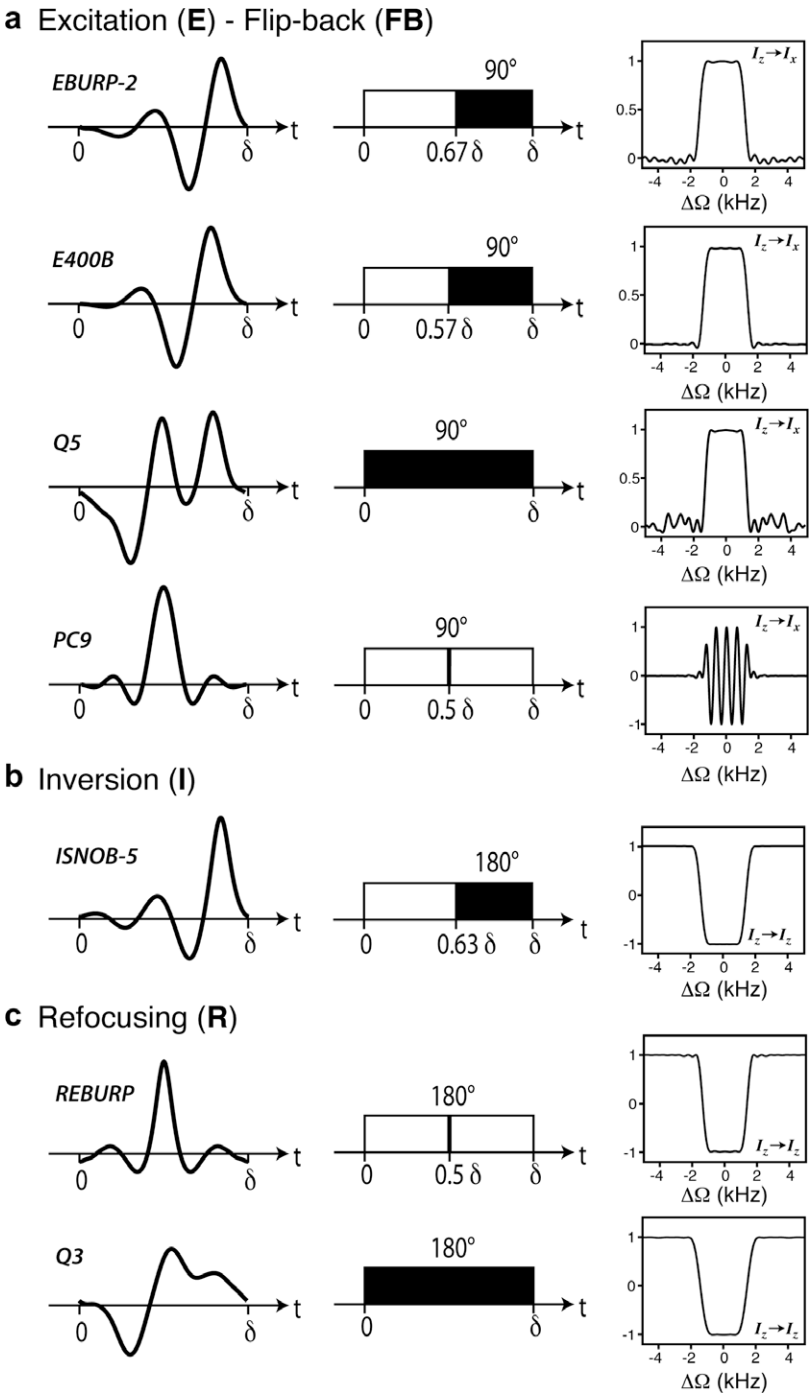

Fig. 2. Amplitude modulation functions, binary schemes with delays optimized by numerical simulations, and excitation (inversion) profiles for several 90° (180°) pulses proposed in the literature. The pulse lengths have been adjusted for an excitation/inversion bandwidth of ±1.2 kHz. (a) Excitation pulse shapes EBURP-2 [5] (δ_E = 1.92 ms, R(0.9 kHz) = 0.14), E400B [17] (δ_E = 1.92 ms, R(0.9 kHz) = 0.15), Q5 [7] (δ_E = 2.31 ms, R(0.9 kHz) = 0.14), and PC9 [18] (δ_E = 3.0 ms, R(0.9 kHz) = 0.11); (b) the inversion pulse ISNOB-5 [8] (δ_E = 1.88 ms, R(0.9 kHz) = 0.06); (c) the refocusing pulses REBURP [5] (δ_E = 2.03 ms, R(0.9 kHz) = 0.09), and Q3 [7] (δ_E = 1.50 ms, R(0.9 kHz) = 0.16). In the case of the refocusing pulses, the binary schemes are valid in presence and in absence of a centered ^{15}N high-power inversion pulse. Note that the ISNOB-5 pulse shape is very similar to IBURP [5].

reversed excitation pulse is commonly used for flip-back (FB) purposes ($I_{xy} \rightarrow I_z$). Time reversal of the pulse shape obviously also translates to a time reversal of the corresponding binary scheme shown in Fig. 2a. As illustrated for the example of excitation pulses EBURP-2 and E400B, both having very similar shapes, only slight changes in the amplitude modulation profile may translate into a significant effect on the binary replacement scheme (different λ-values). Finally, our numerical simulations show that pulse shapes optimized for the same purpose, e.g. the refocusing pulses REBURP and Q3 may show a completely different behavior with respect to hetero-nuclear coupling evolution during the pulse. In absence of an additional ^{15}N 180° pulse, the net effect on ^{1}H chemical shift and hetero-nuclear coupling evolution is essentially the same for the 2 pulse shapes (data not shown). The difference comes into play when a ^{15}N 180° pulse is applied in the middle of the shaped pulse that restores effective hetero-nuclear coupling evolution.

While in the case of the symmetric REBURP shape, hetero-nuclear coupling is effectively active during the entire pulse length ($\lambda \approx 1$), the asymmetric Q3 pulse shape is best described by a single 180° rotation without any hetero-nuclear coupling evolution ($\lambda \approx 0$). This different behavior can be rationalized by a completely different low and high rf-field distribution in REBURP and Q3 pulse shapes (Fig. 2c).

The overall agreement between the spin evolution predicted for the pulse shapes shown in Fig. 2 and their binary representations is astonishingly good within the bandwidth of the shaped pulse. Therefore such simplified schemes present a convenient tool for using the corresponding shaped pulses for various purposes, others than for what they have been initially conceived, in complex multi-pulse sequences. However, except for the refocusing pulse shapes REBURP and Q3, all binary schemes have been derived in the absence of additional rf pulses other than the ^{1}H shaped pulse. Therefore, care should be taken when using these binary schemes in situations where ^{1}H excitation or inversion pulses are applied simultaneously with ^{15}N pulses. With the binary schemes of Fig. 2 in hand, it becomes straightforward to replace hard rf pulses in common pulse sequence elements by the appropriate band-selective pulse shapes, as we will demonstrate in the remaining of this article. As a first example, different experimental realizations of a ^{1}H band-selective hetero-nuclear INEPT transfer are shown in Fig. 3a–d. As demonstrated by numerical simulations, all of these INEPT schemes yield a similar performance with respect to the resulting transfer amplitudes as long as the transfer delays are properly adjusted in order to take into account spin-coupling evolution during the different pulse shapes as given by the corresponding replacement scheme. In particular, it does not matter whether spin excitation is realized by an excitation or flip-back pulse shape (Fig. 3a and b), or whether an inversion or refocusing pulse shape is used for general 180° rotation purposes (Fig. 3d). However, the choice of the shaped pulses has an influence on the overall duration of the INEPT sequence. For example, the band-selective pulse sequence of Fig. 2b is only slightly longer than its standard hard-pulse counterpart as most of the shaped pulse durations are constructively exploited for coherence transfer purposes.

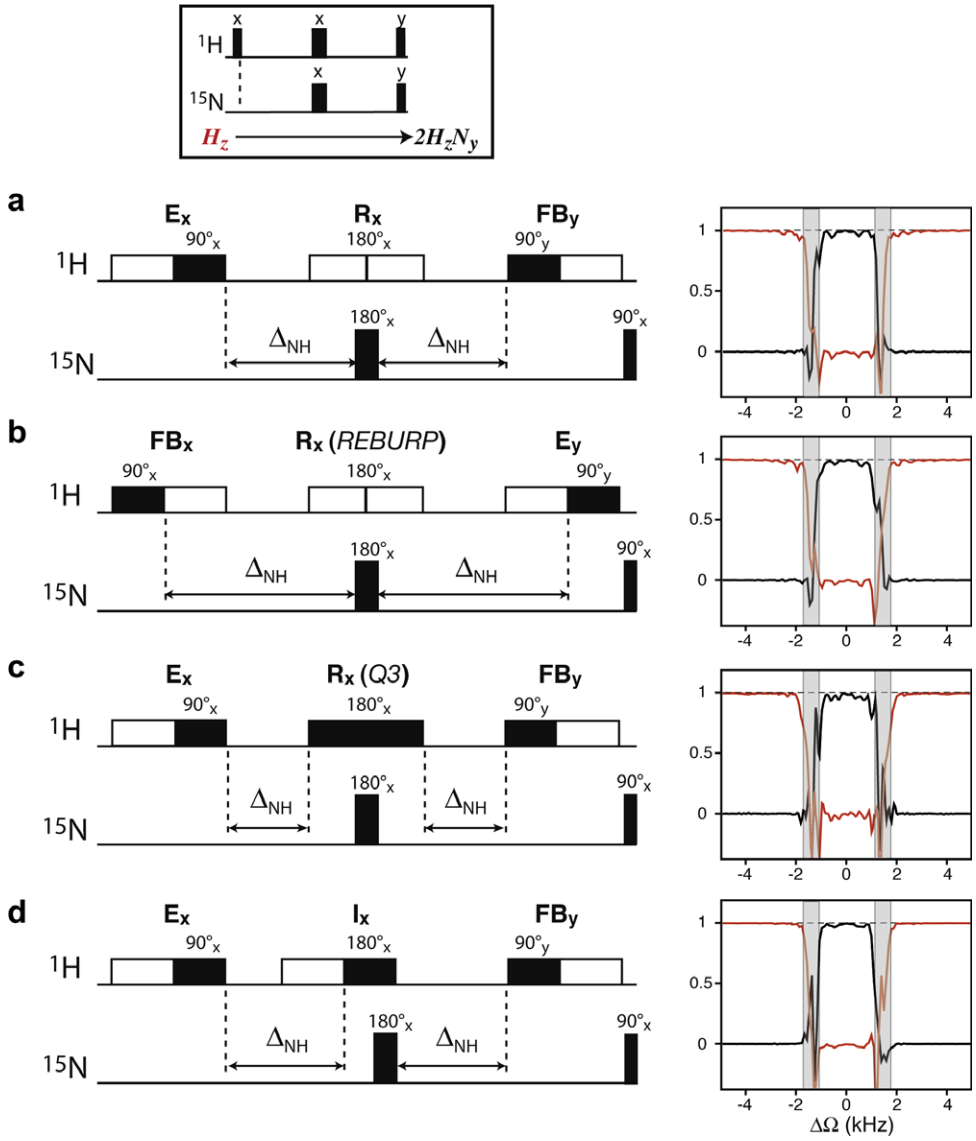

Fig. 3. Experimental realizations of a hetero-nuclear ^{1}H–^{15}N INEPT transfer using different band-selective ^{1}H pulse shapes, and transfer delays adjusted according to the binary schemes introduced in Fig. 1. For all sequences, the initial spin state was H_z and the transfer amplitudes for the $H_z \rightarrow H_z$ (red) and for the $H_z \rightarrow 2H_zN_y$ (black) pathways computed as a function of ^{1}H resonance offset are shown on the right side. (For interpretation of the references to color in this figure legend, the reader is referred to the web version of this article.)

This demonstrates that the use of (relatively) long shaped pulses in biomolecular NMR experiments does not necessarily translate into longer pulse sequences and additional relaxation-induced signal loss, making such BEST-type sequences also of interest for larger fast-relaxing molecular systems.

Let us now discuss more complex pulse schemes where two, or even more coherence–transfer pathways have to be realized at the same time. Fig. 4 shows the experimental realization of a sensitivity-enhanced $^{15}N \rightarrow {}^{1}H$ transfer element required for the preservation of equivalent pathways (PEP) [19], and implemented for echo/antiecho-type ^{15}N quadrature detection in ^{1}H–^{15}N HSQC-type experiments [20]. This sequence, referred to in the following as *planar mixing* scheme [21], converts the 2 orthogonal antiphase coherences $2N_xH_z$ and $2N_yH_z$, present after the ^{15}N chemical shift editing (t_1) period, into detectable ^{1}H inphase coherence H_x and H_y, respectively. As a consequence of the simultaneous occurrence of the two coherence–transfer pathways, each of the 90° ^{1}H pulses (except for the first one) needs to perform 90° spin rotations for two orthogonal spin components, and hetero-nuclear spin-coupling evolution during the pulses cannot be neglected. The pulse sequence of Fig. 4b shows one possible solution to this problem that is based on the use of excitation, flip-back, and refocusing pulse shapes only, and does not require any general 90° rotation pulse. Numerical simulations, shown in Fig. 4c, illustrate the good performance of this pulse scheme with respect to the transfer amplitudes obtained for the two coherence–transfer pathways. It should be pointed out that ^{15}N chemical shift evolves during the whole duration (δ_E) of the first excitation pulse (E_y), while ^{1}H–^{15}N scalar-coupling evolution only occurs during a fraction $\lambda\delta_E$ (with $\lambda = 0.67$ in the case of EBURP-2). Therefore the 180° ^{15}N and ^{1}H pulses are applied after the t_1 period with the delays between them properly adjusted to refocus the two effects (Fig. 4b). A band-selective double-S^{3}CT sequence [22,23] that performs spin-state-selective $^{15}N \rightarrow {}^{1}H$ transfer is shown in Fig. 5a. Again, 2 coherence–transfer pathways need to be realized to convert a ^{15}N single-transition state into a ^{1}H single-transition state. Transfer amplitudes close to 1 are achieved for both pathways (see Fig. 5c) when correctly taking into account spin evolution during the shaped pulses as easily done on the basis of the binary representations presented in Fig. 2.

The band-selective INEPT, planar mixing, and double-S^{3}CT pulse schemes presented in Figs. 3–5, respectively, form the basis of the recently introduced sensitivity-enhanced BEST-HSQC [10,11] and BEST-TROSY [12] experiments that offer new NMR tools for fast and sensitivity-enhanced collection of protein and nucleic acids spectra. In our original work, the various transfer delays were adjusted empirically for optimal sensitivity of the pulse schemes. The resulting values were close, but not identical to the theoreti-

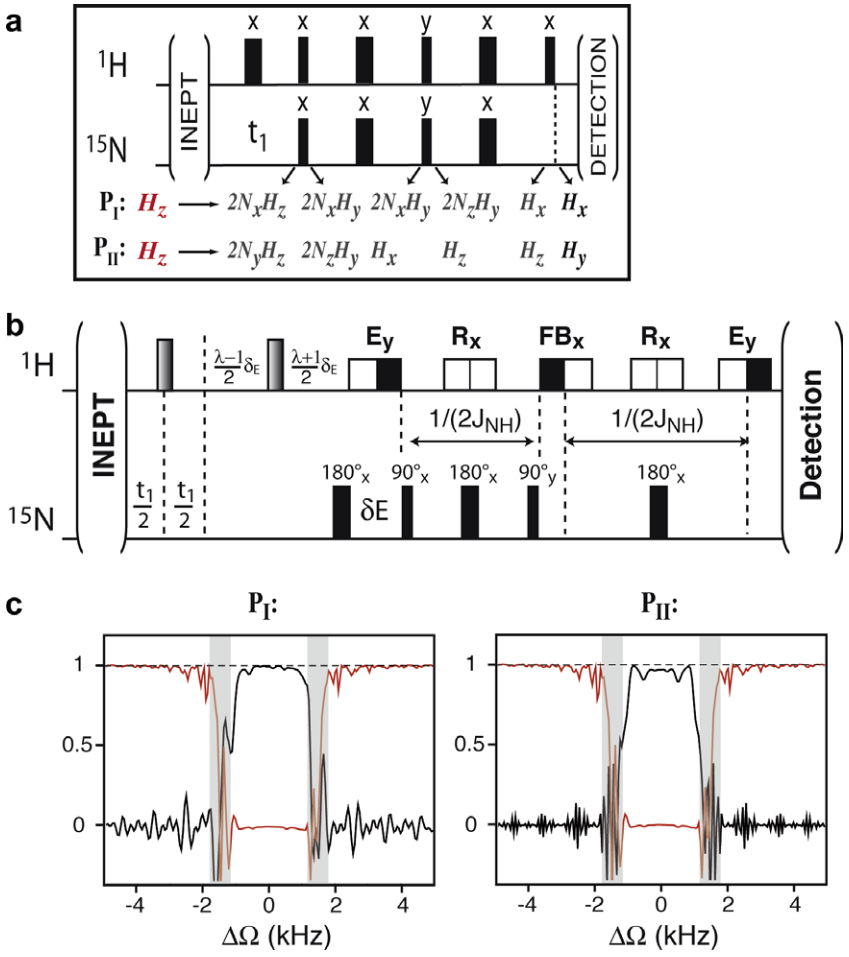

Fig. 4. (a) Planar mixing sequence as required for sensitivity-enhanced ^{15}N–^{1}H back-transfer in HSQC-type correlation experiments. (b) Band-selective version based on excitation, flip-back and refocusing pulse shapes, and optimized transfer delays. The notation δ_E stands for the length of the ^{1}H excitation pulse shape (E), while the scaling factor $\lambda\delta_E$ corresponds to the fraction of the pulse duration that needs to be taken into account for spin coupling and ^{1}H chemical shift evolution according to the schemes of Fig. 2. The ^{1}H 180° pulses applied during the t_1 period are preferably applied with a shape optimized for broad-band spin inversion [25] (c) Amplitude profiles of the initial (red lines) and final (black lines) spin states of the two coherence–transfer pathways computed as a function of ^{1}H resonance offset. (For interpretation of the references to color in this figure legend, the reader is referred to the web version of this article.)

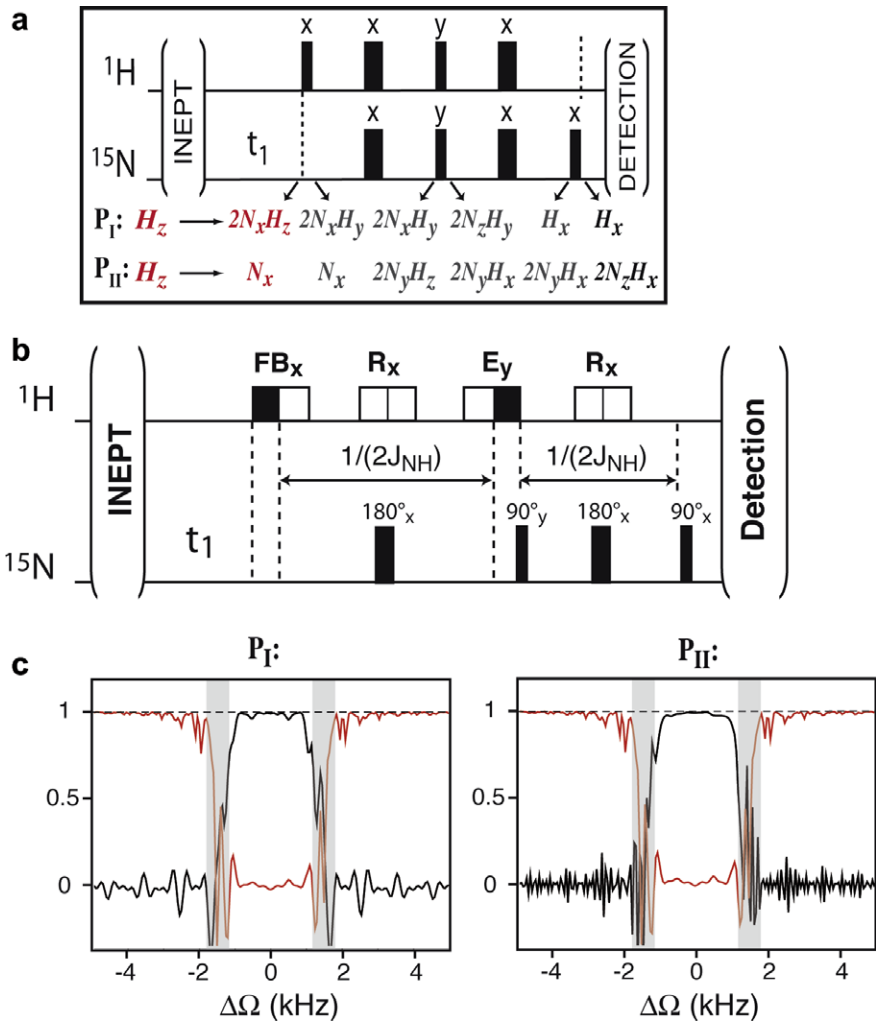

Fig. 5. (a) Double-S^{3}CT sequence as required for single-transition-state-selective ^{15}N–^{1}H back-transfer in TROSY-type correlation experiments. (b) Band-selective version based on excitation, flip-back and refocusing pulse shapes, and optimized transfer delays. (c) Amplitude profiles of the initial (red lines) and final (black lines) spin states of the two coherence–transfer pathways computed as a function of ^{1}H resonance offset. (For interpretation of the references to color in this figure legend, the reader is referred to the web version of this article.)

cally determined optimal values reported here. Therefore, although we could demonstrate the good experimental performance of these sequences, a detailed understanding of the spin evolution during the shaped pulses used in these sequences was still missing. The binary schemes, obtained from numerical simulations and presented here for various band-selective pulse shapes now provide a convenient way for choosing the appropriate pulse shape for a given situation, and for adjusting pulse sequence delays without the need for experimental optimization. Fig. 6 shows an experimental characterization and comparison of ^{1}H–^{15}N sensitivity-enhanced BEST-HSQC and BEST-TROSY correlation experiments. NMR data were recorded for different ^{15}N-labeled, and fully protonated protein samples, ubiquitin (8.6 kDa, 2 mM), β2-microglobulin (12 kDa, 0.3 mM), and YajG (21 kDa, 0.2 mM), on a 600 MHz Varian spectrometer equipped with a cryogenically cooled triple-resonance probe and pulsed z-field gradients. EBURP-2, time-reversed EBURP-2 and REBURP pulses were used for excitation (E), flip-back (FB), and refocusing (R) purposes, as in our hands this combination gave the best results. The experimental sensitivity, defined as the spectral intensity normalized for a given experimental time and equal noise level, has been determined experimentally as a function of the scan time, and is plotted in Fig. 6a for BEST-HSQC, and in Fig. 6b for BEST-TROSY. The scan time comprises the pulse sequence duration including the detection period, as well as the recycle delay. A similar behavior is found for all three proteins with an optimal scan time of ~0.5 s for BEST-HSQC, and a slightly reduced value of ~0.4 s for BEST-TROSY. These optimal scan times, for which the pulse sequences yield highest sensitivity, seem to be independent of the protein size, indicating that the increased ^{1}H spin-diffusion efficiency for larger proteins does not significantly further reduce the selective T_1 relaxation times of amide protons. The slightly shorter optimal scan time found for BEST-TROSY is most likely explained by the smaller number of required ^{1}H pulses in this sequence yielding less disturbance of non-amide protons, and the absence of ^{15}N decoupling during data acquisition that may result in partial probe detuning at high repetition rates [24]. 2D BEST-HSQC spectra (left panel – black contours) and BEST-TROSY spectra (right panel – red contours) recorded under optimal sensitivity conditions are shown for ubiquitin (Fig. 6c), β2-microglobulin (Fig. 6d), and YajG (Fig. 6e). While for ubiquitin the BEST-HSQC yields a slightly higher sensitivity than the BEST-TROSY, for the other proteins the sensitivity obtained by the two BEST pulse schemes is comparable as illustrated by the 1D traces shown on the left of Figs. 6c–e. Because for an amide ^{1}H–^{15}N spin pair the CSA-dipolar cross-correlation becomes more efficient at higher magnetic field strength, with a maximum reached at about

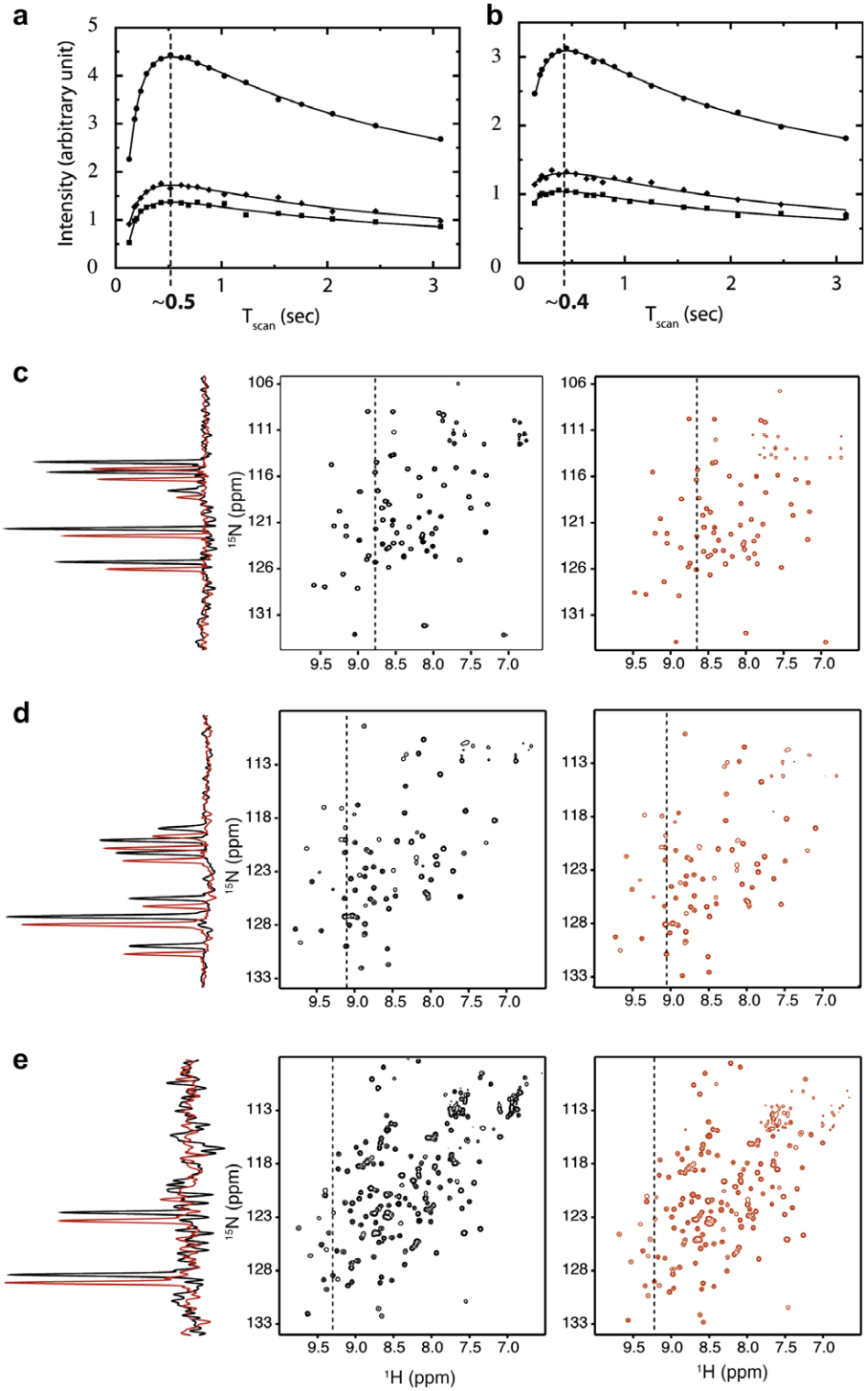

Fig. 6. Experimental data recorded for three different proteins on a 600 MHz Varian spectrometer equipped with a triple-resonance cold probe. Sensitivity curves obtained from a series of (a) 1D BEST-HSQC, and (b) 1D BEST-TROSY spectra. For the initial INEPT transfer the pulse sequence of Fig. 2a was used, and for the back-transfer the sequences of Fig. 4 (HSQC) and Fig. 5 (TROSY) were used as described. The pulse shapes EBURP-2, time-reversed EBURP-2, and REBURP were applied for excitation (E), flip-back (FB), and refocusing (R), respectively. The integrated spectral intensities, normalized for equal measurement times and scan number are plotted as a function of scan time (pulse sequence duration including acquisition time plus recycle delay) for ubiquitin (circles), β2-microglobulin (diamonds), and YajG (squares). 2D BEST-HSQC (left – black contours) and BEST-TROSY (right – red contours) are shown in (a) for ubiquitin, (b) for β2-microglobulin, and (c) for YajG. For all experiments the ^{1}H acquisition time was set to 70 ms, and 100 complex t_1 points were recorded for a ^{15}N spectral width of 1800 Hz. The recycle delay was set to 0.43 s for HSQC and 0.33 s for TROSY experiments. In addition 1D ^{15}N traces extracted at the ^{1}H frequency indicated by a dashed line in the 2D spectra are shown.

1–1.2 GHz ^{1}H frequency, it is expected that at highest currently available magnetic field strength (800 to 1000 MHz) the BEST-TROSY experiment outperforms the BEST-HSQC sequence both in terms of sensitivity and spectral resolution. Typically a 30–100% sensitivity gain is achieved for (protonated) proteins or nucleic acids when using ^{1}H–^{15}N BEST-type experiments instead of

standard hard-pulse-based pulse sequences if both are optimized independently for optimal sensitivity [10–12]. Of course, these BEST sequence blocks (Figs. 2–4) are equally useful for higher-dimensional triple-resonance H–N–C type correlation experiments to increase experimental sensitivity or to reduce experimental times.

In conclusion, we have introduced simplified schemes for various amplitude-modulated pulse shapes commonly used for band-selective spin manipulation in NMR experiments of macromolecules. These binary schemes, consisting in a suite of evolution delays and ideal rf pulses, enable easy use of such pulse shapes in the conception of complex multi-pulse sequences, and ensure their optimal performance, as demonstrated here for longitudinal-relaxation-enhanced $^{1}H–^{15}N$ BEST-HSQC and BEST-TROSY experiments.

References

[1] O.W. Sørensen, G.W. Eich, M.H. Levitt, G. Bodenhausen, R.R. Ernst, Product operator-formalism for the description of NMR pulse experiments, Prog. NMR Spectrosc. 16 (1983) 163–192.

[2] K. Pervushin, B. Vögeli, A. Eletsky, Longitudinal H-1 relaxation optimization in TROSY NMR spectroscopy, J. Am. Chem. Soc. 124 (2002) 12898–12902.

[3] P. Schanda, B. Brutscher, Very fast two-dimensional NMR spectroscopy for real-time investigation of dynamic events in proteins on the time scale of seconds, J. Am. Chem. Soc. 127 (2005) 8014–8015.

[4] P. Schanda, Fast-pulsing longitudinal relaxation optimized techniques: enriching the toolbox of fast Biomolecular NMR spectroscopy, Prog. NMR Spectrosc. 55 (2009) 238–265.

[5] H. Geen, R. Freeman, Band-selective radiofrequency pulses, J. Magn. Reson. 93 (1991) 93–141.

[6] L. Emsley, G. Bodenhausen, Gaussian pulse cascades – new analytical functions for rectangular selective inversion and in-phase excitation in NMR, Chem. Phys. Lett. 165 (1990) 469–476.

[7] L. Emsley, G. Bodenhausen, Optimization of shaped selective pulses for NMR using a quaternion description of their overall propagators, J. Magn. Reson. 97 (1992) 135–148.

[8] E. Kupce, J. Boyd, I.D. Campbell, Short selective pulses for biochemical applications, J. Magn. Reson. B 106 (1995) 300–303.

[9] N.I. Gershenzon, T.E. Skinner, B. Brutscher, N. Khaneja, M. Nimbalkar, B. Luy, S.J. Glaser, Linear phase slope in pulse design: application to coherence transfer, J. Magn. Reson. 192 (2008) 235–243.

[10] P. Schanda, H. Van Melckebeke, B. Brutscher, Speeding up three-dimensional protein NMR experiments to a few minutes, J. Am. Chem. Soc. 128 (2006) 9042–9043.

[11] E. Lescop, P. Schanda, B. Brutscher, A set of BEST triple-resonance experiments for time-optimized protein resonance assignment, J. Magn. Reson. 187 (2007) 163–169.

[12] J. Farjon, J. Boisbouvier, P. Schanda, A. Pardi, J.P. Simorre, B. Brutscher, Longitudinal relaxation enhanced NMR experiments for the study of nucleic acids in solution, J. Am. Chem. Soc. 131 (2009) 8571–8577.

[13] B. Ewing, S.J. Glaser, G.P. Drobny, Development and optimization of shaped NMR pulses for the study of couples spin systems, Chem. Phys. 147 (1990) 121–129.

[14] R. Freeman, Shaped radiofrequency pulses in high resolution NMR, Prog. NMR Spectrosc. 32 (1998) 59–106.

[15] J.M. Nuzillard, Biselective refocusing pulses and the SERF experiment, J. Magn. Reson. 187 (2007) 193–198.

[16] M. Veshtort, R.G. Griffin, SPINEVOLUTION: a powerful tool for the simulation of solid and liquid state NMR experiments, J. Magn. Reson. 178 (2006) 248–282.

[17] M. Veshtort, R.G. Griffin, High-performance selective excitation pulses for solid- and liquid-state NMR spectroscopy, Chemphyschem 5 (2004) 834–850.

[18] E. Kupce, R. Freeman, Optimized adiabatic pulses for wideband spin inversion, J. Magn. Reson. A 118 (1996) 299–303.

[19] A.G. Palmer, J. Cavanagh, P.E. Wright, M. Rance, Sensitivity improvement in proton-detected 2-dimensional heteronuclear correlation NMR-spectroscopy, J. Magn. Reson. 93 (1991) 151–170.

[20] L.E. Kay, P. Keifer, T. Saarinen, Pure absorption gradient enhanced heteronuclear single quantum correlation spectroscopy with improved sensitivity, J. Am. Chem. Soc. 114 (1992) 10663–10665.

[21] T. Schulte-Herbrüggen, Z.L. Madi, O.W. Sørensen, R.R. Ernst, Reduction of multiplet complexity in cosy-type NMR-spectra – the bilinear and planar cosy experiments, Mol. Phys. 72 (1991) 847–871.

[22] K. Pervushin, R. Riek, G. Wider, K. Wüthrich, Attenuated T-2 relaxation by mutual cancellation of dipole–dipole coupling and chemical shift anisotropy indicates an avenue to NMR structures of very large biological macromolecules in solution, Proc. Natl. Acad. Sci. USA 94 (1997) 12366–12371.

[23] A. Meissner, T. Schulte-Herbrüggen, J. Briand, O.W. Sørensen, Double spin-state-selective coherence transfer. Application for two-dimensional selection of multiplet components with long transverse relaxation times, Mol. Phys. 95 (1998) 1137–1142.

[24] T. Kern, P. Schanda, B. Brutscher, Sensitivity-enhanced IPAP-SOFAST-HMQC for fast-pulsing 2D NMR with reduced radiofrequency load, J. Magn. Reson. 190 (2008) 333–338.

[25] M.A. Smith, H. Hu, A.J. Shaka, Improved broadband inversion performance for NMR in liquids, J. Magn. Reson. 151 (2001) 269–283.